ChemPubSoc Europe

DOI: 10.1002/ejic.201600694

EurJIC European Journal of Inorganic Chemistry

Full Paper

Oxygen Atom Transfer

# Dioxidomolybdenum(VI) Complexes of Tripodal Tetradentate Ligands for Catalytic Oxygen Atom Transfer between Benzoin and Dimethyl Sulfoxide and for Oxidation of Pyrogallol

Mannar R. Maurya,*[a] Bhawna Uprety,[a] and Fernando Avecilla[b]

**Abstract:** The reactions of the tripodal tetradentate ONNO donor ligands 6,6′-{[(2-morpholinoethyl)azanediyl]bis(methylene)}bis(2,4-di-*tert*-butylphenol) ($H_2$**L**$^1$), 6,6′-{[(2-morpholinoethyl)azanediyl]bis(methylene)}bis(2,4-dimethylphenol) ($H_2$**L**$^2$) and 6,6′-{[(2-morpholinoethyl)azanediyl]bis(methylene)}bis[2-(*tert*-butyl)-4-methylphenol] ($H_2$**L**$^3$) with [$Mo^{VI}O_2(acac)_2$] (acac = acetylacetonato) in a 1:1 molar ratio in MeOH gave the corresponding *cis*-dioxidomolybdenum(VI) complexes [$MoO_2$(**L**$^1$)], [$MoO_2$(**L**$^2$)] and [$MoO_2$(**L**$^3$)], respectively, in excellent yields. These complexes were characterized by various spectroscopic (IR, UV/Vis, $^1$H and $^{13}$C NMR), electrochemical, thermogravimetric, single-crystal XRD, and powder XRD (PXRD) studies. In these complexes, the geometry around the *cis*-$[MoO_2]^{2+}$ core is distorted octahedral, and the ligands are tetradentate and coordinate through two $O_{phenolate}$, one $N_{tripodal}$, and one $N_{morpholine}$ atoms. One of the oxido groups and the morpholine nitrogen atom occupy the axial sites. These complexes were used for catalytic oxygen atom transfer between benzoin and dimethyl sulfoxide (DMSO) in acetonitrile at 80 °C, and the formation of benzil was followed by HPLC. Detailed kinetic studies revealed a first-order rate in benzoin and catalyst, and the rate constant for the second-order oxygen atom transfer reaction was 0.0162 $M^{-1}$ $h^{-1}$. The formation of the dinuclear intermediates [$LMo^V$–μ-O-$Mo^V$L] was established by MALDI-TOF MS and UV/Vis spectroscopy. Its reversible nature was further supplemented by UV/Vis spectroscopy. These complexes also catalyze the oxidation of pyrogallol in a fashion similar to that of transhydroxylases. Under aerobic conditions, the initially formed oxidation product phloroglucinol undergoes further oxidative coupling in the presence of $H_2O_2$ to give purpurogallin as the final product. This process follows Michaelis–Menten-type kinetics with respect to pyrogallol; the $k_{cat}$ values obtained were 394, 300 and 247 $h^{-1}$ for [$Mo^{VI}O_2$(**L**$^1$)], [$Mo^{VI}O_2$(**L**$^2$)] and [$Mo^{VI}O_2$(**L**$^3$)], respectively.

## Introduction

The second-row transition element molybdenum is vital for all living organisms. It is also an important cofactor for many enzymes, of which at least fifty have been isolated and characterized biochemically.[1,2] Excluding nitrogenases, which contain the multinuclear iron–molybdenum cofactor (FeMoco) as the active site, most other molybdenum-containing oxotransferases are mononuclear and fall into three broad categories depending on their active-site structure, that is, sulfite oxidases, dimethyl sulfoxide reductases, and xanthine oxidases.[3–7] The enzymes containing the molybdenum cofactor (Moco) may be hydroxylases or oxotransferases and catalyze reactions involving the transfer of oxygen to and from the substrate in a two-electron process. Mononuclear molybdenum-based enzymes are crucial to carbon, nitrogen, and sulfur biogeochemical cycles and serve primarily to transfer oxygen atoms to physiological substrates.[8,9] In all of these enzymes, the active form has a $Mo^{IV}$ centre, and the Mo centre shuttles between the VI and IV oxidation states during the catalytic cycle in pyranopterin–dithiolene ligand environments.[10] Notably, an important exclusive property of the Moco active site is its ability to engage in reversible two-electron reduction and oxidation processes cooperatively with a substrate.[11] The oxidation from $Mo^{IV}$ to $Mo^{VI}$ can either be a concerted two-electron process or can involve one-electron transfer steps via $Mo^V$ intermediates.[1]

One of the most explored categories of Mo enzymes is the dimethyl sulfoxide reductases (DMSOR). These constitute the largest and most diverse enzymes of the Moco family.[12] Members of this family are found only in the bacteria and the archaea, and the family contains both molybdenum enzymes and all tungsten enzymes that have been discovered to date.[11] Dimethyl sulfoxide reductases reduce dimethyl sulfoxide (DMSO) to dimethyl sulfide (DMS) along with oxido transfer and the consequent oxidation of $Mo^{IV}$ to $Mo^{VI}$ possibly via a $Mo^V$ intermediate.[7] The active-site structure of a fully oxidized $Mo^{VI}$ DMSO reductase comprises a $Mo^{VI}$ centre coordinated to two pyranopterin cofactors in an $L_2Mo^{VI}Y(X)$ trigonal-prismatic coordination geometry, in which Y is the labile Mo=O group and X is a serinate ligand that completes the metal coordination sphere of the oxidized enzyme.[5–8] Several synthetic models based on the *cis*-$[MoO_2]^{2+}$ core have been proposed and evaluated for their oxygen atom transfer properties and related

[a] *Department of Chemistry, Indian Institute of Technology Roorkee, Roorkee 247667, India*
*E-mail: rkmanfcy@iitr.ac.in*
*www.iitr.ac.in/~CY/rkmanfcy*
[b] *Departamento de Química Fundamental, Universidade da Coruña, Campus de A Zapateira, 15071 A Coruña, Spain*

*Supporting information for this article is available on the WWW under http://dx.doi.org/10.1002/ejic.201600694.*

mechanistic pathways. Most of these studies involve tertiary phosphines as ideal substrates because their properties can be tuned readily by substitution and the reactions can be followed by $^{31}P$ NMR spectroscopy.[13–23] The generally accepted pathway for oxygen atom transfer (OAT) reactions with tertiary phosphines involves an associative mechanism[10,16,20] initiated by the nucleophilic attack of the phosphine onto the more accessible and labile oxido atom, and the other oxido ligand acts as the "spectator group" and serves to strengthen the Mo=O bond through the formation of a formal Mo≡O bond during the oxygen transfer process.[10,13]

The transhydroxylase from *Pelobacter acidigallici* is also a Moco enzyme from the DMSO reductase family that catalyzes the anaerobic conversion of pyrogallol to phloroglucinol with 1,2,3,5-tetrahydroxybenzene as the cocatalyst.[24,25] The overall catalytic process involves a nonredox reaction consisting of a reductive dehydroxylation and an oxidative hydroxylation in two consecutive steps. The Mo coordination in this hydroxylase is closely related to that of DMSO reductase, and, like DMSO, the substrate pyrogallol coordinates directly to the Mo ion.[26]

We have recently explored the catalytic role of *cis*-$[Mo^{VI}O_2]^{2+}$ complexes with ONO/ONS donor ligands in the oxidation and oxidative bromination of various organic substrates mediated by $H_2O_2/NaHCO_3$. Most of these reactions are thought to proceed via an oxidoperoxido intermediate, the formation of which has been substantiated by UV/Vis spectroscopic evidence as well as single-crystal X-ray structures in some cases.[27] In the present study, we have performed a detailed kinetic study and deduced the rate equation for oxygen atom transfer between DMSO and benzoin catalyzed by *cis*-$[MoO_2]^{2+}$ complexes of tripodal tetradentate ligands through high-performance liquid chromatography. We have also confirmed the formation of the dinuclear intermediate $[LMo^{V}–\mu\text{-}O–Mo^{V}L]$ through UV/Vis spectroscopy as well as MALDI-TOF MS analysis. An OAT reaction between benzoin and DMSO at 100 °C catalyzed by *cis*-$[Mo^{VI}O_2]^{2+}$ and *cis*-$[W^{VI}O_2]^{2+}$ complexes was reported by Ng et al.[28,29] Similar studies on benzoin were also reported by Sillanpää et al.[30] However, in all of these cases, the characterization of the product was confirmed by $^1H$ NMR spectroscopy, and no effort was made to identify the intermediate(s). We have also performed peroxidase mimetic studies with pyrogallol as the ideal substrate under aerobic conditions.

## Results and Discussion

Mannich condensations between 2-aminoethylmorpholine, formaldehyde and 2,4-disubstituted phenols in MeOH afforded the analytically pure tripodal ligands $H_2\mathbf{L^{1–3}}$ (Scheme 1). The reactions of $[Mo^{VI}O_2(acac)_2]$ (acac = acetylacetonato) with the dibasic tetradentate tripodal ligands $H_2\mathbf{L^{1–3}}$ in 1:1 molar ratios in MeOH gave the corresponding dioxidomolybdenum(VI) complexes $[Mo^{VI}O_2(\mathbf{L^1})]$·MeOH (**1**), $[Mo^{VI}O_2(\mathbf{L^2})]$ (**2**) and $[Mo^{VI}O_2(\mathbf{L^3})]$ (**3**) in good yields (Scheme 1). Single-crystal X-ray analysis indicates a distorted octahedral Mo centre in all complexes. All of the complexes are air-stable yellow solids that are soluble in MeCN, DMSO and *N*,*N*-dimethylformamide (DMF) and sparingly soluble in MeOH and EtOH.

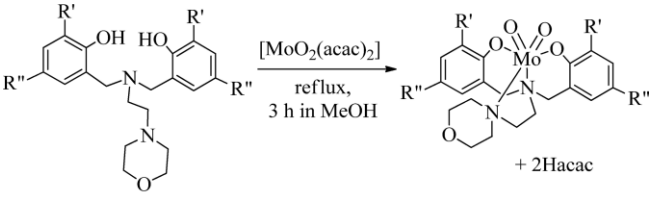


| R′ | R″ | Ligand | Complex |
|---|---|---|---|
| *tert*-butyl | *tert*-butyl | $H_2L^1$ | $[Mo^{VI}O_2(L^1)]$ |
| methyl | methyl | $H_2L^2$ | $[Mo^{VI}O_2(L^2)]$ |
| *tert*-butyl | methyl | $H_2L^3$ | $[Mo^{VI}O_2(L^3)]$ |

Scheme 1. Synthesis of *cis*-$[Mo^{VI}O_2]^{2+}$ complexes.

### Description of the Structures of the Complexes

ORTEP diagrams for **1**–**3** are shown in Figures 1, 2 and 3, respectively. Selected bond lengths and angles are given in Table 1.

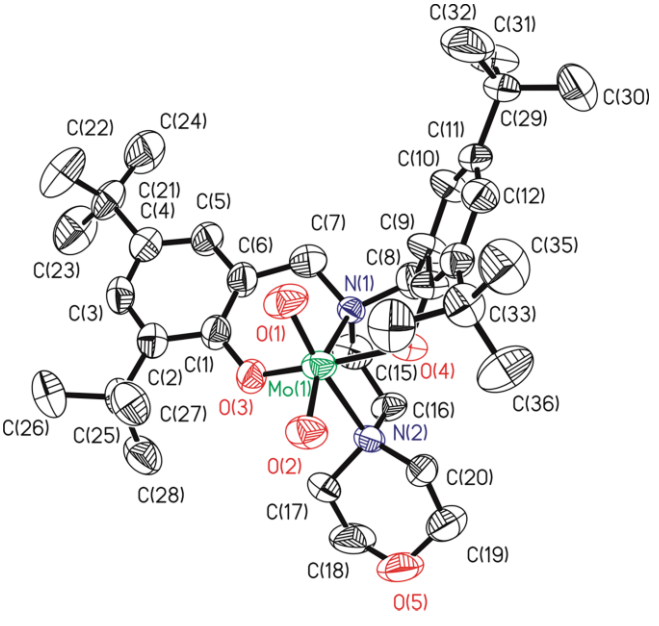


Figure 1. ORTEP plot of $[Mo^{VI}O_2(L^1)]$·MeOH (**1**). All non-hydrogen atoms are represented by their 50 % probability ellipsoids. Hydrogen atoms are omitted for clarity.

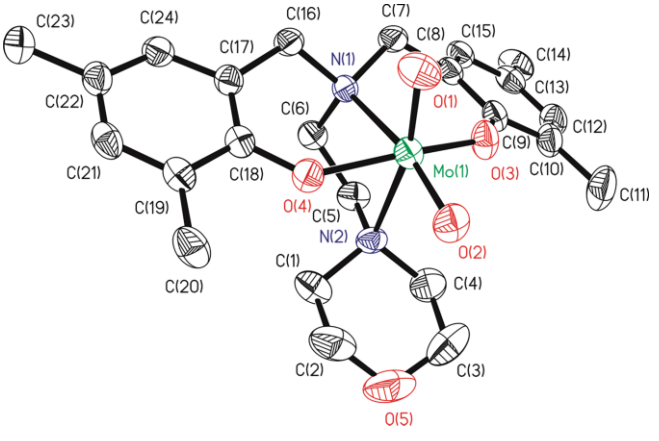


Figure 2. ORTEP plot of $[Mo^{VI}O_2(L^2)]$ (**2**). All non-hydrogen atoms are represented by their 50 % probability ellipsoids. Hydrogen atoms are omitted for clarity.

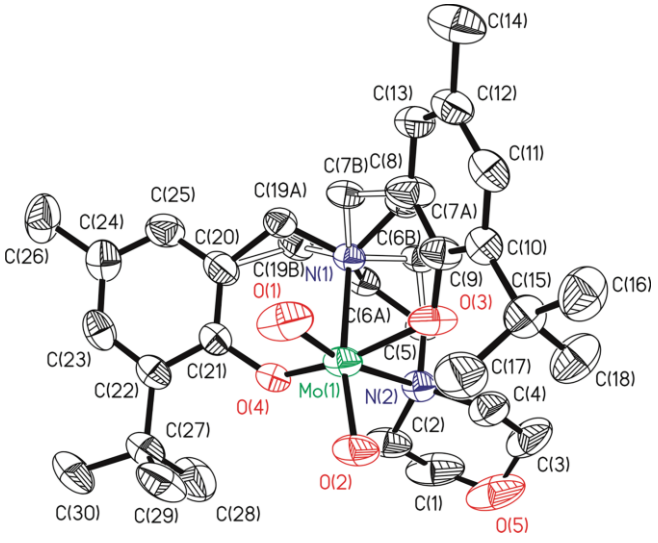


Figure 3. ORTEP plot of $[Mo^{VI}O_2(L^3)]$ (**3**). All non-hydrogen atoms are represented by their 50 % probability ellipsoids. Hydrogen atoms are omitted for clarity.

Table 1. Bond lengths [Å] and angles [°] for **1**–**3**.

| Bond lengths | 1 | 2 | 3 |
|---|---|---|---|
| Mo(1)–O(1) | 1.699(4) | 1.694(2) | 1.694(3) |
| Mo(1)–O(2) | 1.699(4) | 1.707(2) | 1.705(3) |
| Mo(1)–O(3) | 1.938(4) | 1.927(2) | 1.944(3) |
| Mo(1)–O(4) | 1.960(4) | 1.921(2) | 1.941(3) |
| Mo(1)–N(1) | 2.381(4) | 2.393(2) | 2.371(3) |
| Mo(1)–N(2) | 2.466(5) | 2.577(3) | 2.462(4) |
| **Angles** | **1** | **2** | **3** |
| O(1)–Mo(1)–O(2) | 107.6(2) | 106.66(12) | 108.42(15) |
| O(1)–Mo(1)–O(3) | 95.2(2) | 98.52(11) | 96.03(18) |
| O(2)–Mo(1)–O(3) | 98.76(19) | 96.54(11) | 98.71(14) |
| O(1)–Mo(1)–O(4) | 95.4(2) | 97.62(11) | 96.20(18) |
| O(2)–Mo(1)–O(4) | 98.76(19) | 96.21(10) | 97.97(14) |
| O(3)–Mo(1)–O(4) | 155.73(16) | 155.60(10) | 155.01(16) |
| O(1)–Mo(1)–N(1) | 95.52(17) | 88.61(10) | 90.54(14) |
| O(2)–Mo(1)–N(1) | 156.83(17) | 164.67(10) | 161.03(14) |
| O(3)–Mo(1)–N(1) | 77.10(15) | 82.12(9) | 79.31(12) |
| O(4)–Mo(1)–N(1) | 80.18(15) | 80.10(9) | 78.86(12) |
| O(1)–Mo(1)–N(2) | 168.51(17) | 161.87(10) | 165.12(14) |
| O(2)–Mo(1)–N(2) | 83.89(17) | 91.46(10) | 86.46(13) |
| O(3)–Mo(1)–N(2) | 82.42(16) | 80.18(9) | 80.99(13) |
| O(4)–Mo(1)–N(2) | 82.88(15) | 78.76(9) | 81.60(13) |
| N(1)–Mo(1)–N(2) | 72.98(14) | 73.26(8) | 74.58(11) |

Complexes **1**, **2** and **3** adopt distorted six-coordinate octahedral geometries in which the ligands are tetradentate and coordinate through two $O_{phenolate}$, one $N_{tripodal}$ and one $N_{morpholine}$ atoms. The coordination sphere of the Mo centre is completed by bonds to two terminal oxido ligands. The axial sites are occupied by the oxido group O(1) and by the nitrogen atoms N(2) of the morpholine group. The equatorial plane is formed by three atoms of the ligand [N(1), O(3) and O(4)] and one of the terminal oxygen atoms, O(2), and is distorted slightly from planarity [mean deviations from the plane for N(1), O(2), O(3) and O(4): 0.0960(20) Å in **1**, 0.0221(12) Å in **2** and 0.0371(18) Å in **3**]. The molybdenum atoms are displaced toward the apical oxido ligand, O(1), from the equatorial plane defined by the O(2), O(3), O(4) and N(1) atoms by 0.3012(20) Å in **1**, 0.2870(11) Å in **2** and 0.2893(19) Å in **3**. The Mo–$O_{oxido}$ bond lengths [Mo(1)–O(1): 1.699(4) Å in **1**, 1.694(2) Å in **2** and 1.695(3) Å in **3**; and Mo(1)–O(2): 1.699(4) Å in **1**, 1.707(2) Å in **2** and 1.703(3) Å in **3** (see Table 1)] and bond angles [O=Mo=O: 107.6(2)° in **1**, 106.66(12)° in **2** and 108.42(15)° in **3**] are within the ranges typically observed in this type of compound.[31] The Mo–$N_{tripodal}$ distances are long in the three complexes (see Table 1). This is possibly caused by the strong *trans* effect of the oxido ligands. In the same way, the Mo–$O_{phenolate}$ distances are in a range [1.921(2)–1.960(4) Å] similar to those reported for other $Mo^{VI}$–$N_{tripodal}$ $Mo^{VI}$–$O_{phenolate}$ complexes.[31b] No π–π stacking interactions or hydrogen bonds were observed in the crystal packing of these complexes.

## Powder XRD Studies

The bulk purity of the synthesized dioxidomolybdenum complexes was supported by their powder X-ray diffraction patterns (Figure S1a–c). The peaks for the synthesized compounds are in good agreement with the simulated peaks obtained from the single-crystal data; therefore, the single crystals are representative of the bulk materials.

## IR Spectroscopy Studies

The broad peak in the IR spectra of all of the ligands at $\tilde{\nu} \approx 3400$ $cm^{-1}$ owing to the phenolic –OH group vanishes in the spectra of the complexes; therefore, the oxygen atom is coordinated following deprotonation. The sharp peaks arising at $\tilde{\nu} = 900–950$ $cm^{-1}$ are attributed to the characteristic $\nu(MoO_2)$ symmetric and asymmetric stretches. The spectra also include stretching frequencies at $\tilde{\nu} \approx 2800–3000$ $cm^{-1}$ for the different alkyl groups.

## UV/Vis Spectroscopy Studies

The UV/Vis spectra of the prepared ligands and their corresponding metal complexes in MeCN were recorded, and the relevant data are presented in Table 2 and Figures S2–S4. The spectra of all the three ligands are identical, and present two bands at $\lambda = 225–234$ and 282–285 nm corresponding to intraligand π→π* and n→π* transitions, respectively. All of these bands are also present in the spectra of the metal complexes with slight shifts in wavelengths owing to complex formation.

Table 2. UV/Vis data for the prepared ligands and complexes.

| Entry | Compound | λ [nm] (ε, $M^{-1}$ $cm^{-1}$) |
|---|---|---|
| 1 | $H_2L^1$ | 234 ($9.3 \times 10^3$), 282 ($4.2 \times 10^3$) |
| 2 | $H_2L^2$ | 225 ($1.5 \times 10^4$), 285 ($5.1 \times 10^3$) |
| 3 | $H_2L^3$ | 231 ($1.1 \times 10^4$), 284 ($5.1 \times 10^3$) |
| 4 | **1** | 235 ($2.1 \times 10^4$), 279 ($8.2 \times 10^3$), 373 ($2.9 \times 10^3$) |
| 5 | **2** | 236 ($2.1 \times 10^4$), 278 ($7.3 \times 10^3$), 358 ($5.7 \times 10^3$) |
| 6 | **3** | 235 ($1.9 \times 10^3$), 280 ($7.9 \times 10^3$), 379 ($2.7 \times 10^3$) |

Additionally, the spectra of all of the complexes display an intense charge-transfer band at $\lambda$ = 358–379 nm.

### $^1$H and $^{13}$C NMR Spectroscopy Studies

The coordination mode of the ligands was further ascertained by recording the $^1$H NMR spectra of all the three ligands and their respective *cis*-$[Mo^{VI}O_2]^{2+}$ complexes in [$D_6$]DMSO. The spectra for $H_2$**L$^2$** and **2** as the representative spectra for the ligands and *cis*-$[Mo^{VI}O_2]^{2+}$ complexes under study are presented in Figure 4.

The broad signal at $\delta$ = 9.45–9.64 ppm in the spectra of the three ligands is attributed to the two phenolic –OH protons. The disappearance of this signal in the spectra of the complexes indicates the coordination of the O atom after deprotonation. The effect of coordination is very pronounced on the protons in the vicinity of the coordinating atoms. Thus, the methylenic protons between the tripodal nitrogen atom and the phenolic rings appear as a singlet at $\delta$ = 3.5 ppm in the ligand spectra, whereas this signal splits into two doublets in the spectra of all complexes and appears at slightly higher $\delta$ values. This behaviour is quite common for metal complexes bearing tripodal ligands.[32] Similarly, the two adjacent methylene protons between the tripodal nitrogen atom and the morpholine ring also become diastereotopic following coordination and appear as two distinct triplets at higher $\delta$ values owing to the coordination of the morpholine nitrogen atom. The protons of the morpholine ring also unveil the influence of coordination. Thus, the well-defined signals of the morpholine ring in the spectra of the ligands cluster into multiplets in the complexes (see Figures S5 and S6 for **1** and **3**, respectively) upon coordination and become downshielded in **2** (Figure 4). The aromatic protons and the alkyl groups resonate within the expected regions. The $^{13}$C NMR spectra of all the ligands along with possible assignments are presented in Table S1 and Figures S7–S9. Unfortunately, we could not obtain the $^{13}$C NMR spectra of **1**–**3** owing to their poor solubility in suitable deuterated solvents.

### Thermogravimetric Analysis

The thermogravimetric analysis of the dioxidomolybdenum(VI) complexes was performed between room temperature and 700 °C at a heating rate of 10 °C min$^{-1}$ under an oxygen atmosphere (Figure S10). All of the complexes are stable and do not lose any weight up to ca. 280 °C. Further temperature increases cause decomposition of the complexes in two overlapping steps. The first step ranges from 278–308 °C for **1**, 282–300 °C for **2** and 280–305 °C for **3**, and the second step completes with the formation of $MoO_3$ at ca. 700 °C for the three complexes. The observed weight-loss values of 19.3 % for **1**, 26.6 % for **2**, and 23.5 % for **3** are close to the calculated values of 20.7, 27.4, and 23.6 %, respectively. The estimation of the loss of particular ligand fragments during the whole analysis process was not possible.

### Oxotransfer Activity and Electrochemistry

The kinetics of the oxygen atom transfer between DMSO and benzoin have mainly been studied through $^1$H NMR spectroscopy.[28–30] We have used HPLC and performed the catalytic OAT reactions between benzoin and DMSO in acetonitrile. The reaction was performed over 24 h, and the decrease in the concentration of benzoin and the formation of benzil with time were measured periodically by HPLC with a water/acetonitrile/

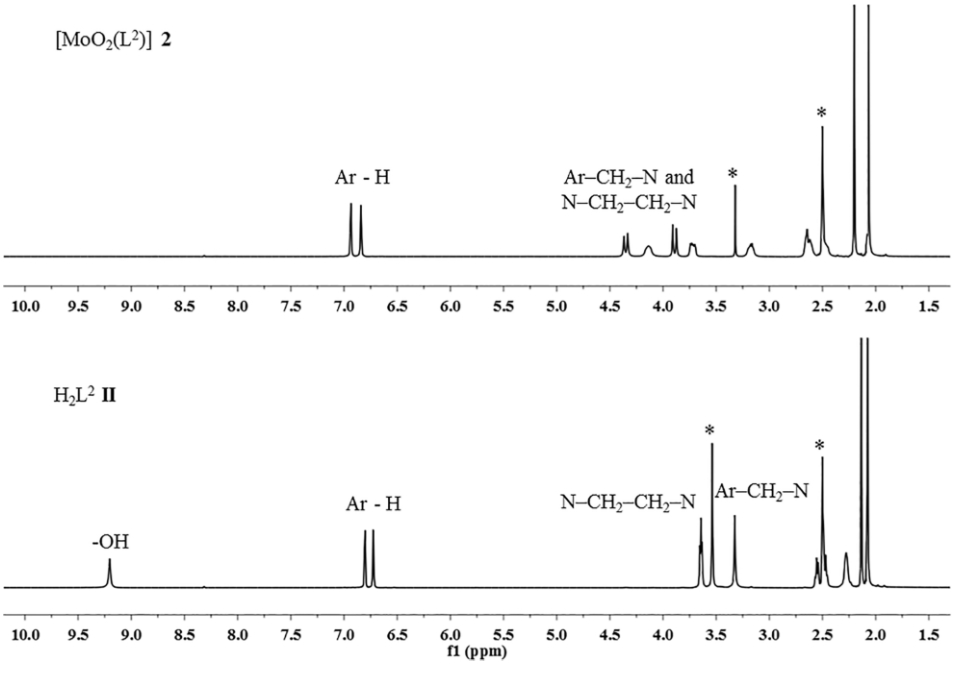


Figure 4. $^1$H NMR spectra of $H_2$**L$^2$** and **2** in [$D_6$]DMSO; * indicates the proton impurity signal present in [$D_6$]DMSO at $\delta$ = 2.5 ppm and that of moisture at $\delta$ = 3.5 ppm.

trifluoroacetic acid (MeCN/$H_2O$/TFA) mixture (60:40:02) as the eluent (Figure 5). The selective formation of benzil was observed.

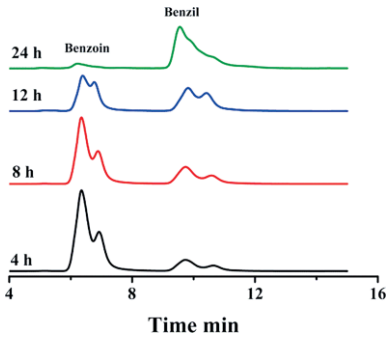


Figure 5. The reaction progress, as monitored by HPLC analysis of the reaction mixture at different time intervals. Mobile phase: MeCN/$H_2O$/TFA 60:40:0.02 (for details, see text. The two peaks observed for both benzoin and benzil are caused by two isomers in each case).

To optimize the reaction parameters such as catalyst amount and reaction temperature to achieve the maximum conversion of benzoin (1.06 g, 5 mmol) in the presence of an excess of DMSO, **2** was chosen as the representative catalyst. Thus, three parallel reactions were performed at temperatures of 60, 70 and 80 °C for benzoin (5 mmol) with **2** (0.0010 g, 1.9 μmol) and DMSO (1 mL) in MeCN (10 mL). As shown in Figure 6 (a), the temperature increase improved the conversion significantly; the best conversion (38 %) was obtained at 80 °C after 24 h of reaction time, whereas the lower reaction temperatures gave poor conversions. Thus, 80 °C was chosen as the optimum temperature for the OAT reaction between benzoin and DMSO.

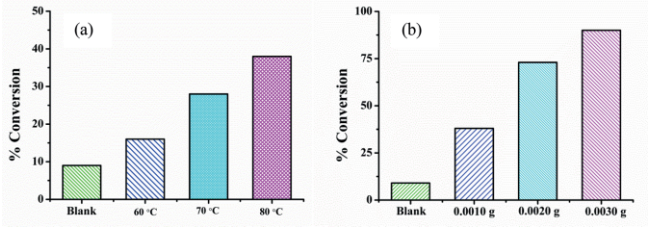


Figure 6. OAT between benzoin and DMSO catalyzed by **2**: effect of (a) temperature and (b) catalyst amount on the overall conversion [%] of benzoin (5 mmol; for detail, see text).

The effect of the amount of catalyst on the rate of the reaction at 80 °C for benzoin (5 mmol) was evaluated with three different amounts of catalyst [0.0010 (1.9 μmol), 0.0020 (3.8 μmol) and 0.0030 g (5.7 μmol)] with all other parameters kept as stated above. The obtained results are summarized in Figure 6b and Table 3. The increasing catalyst amount improved the reaction rates, and the best conversion (90 %) was achieved with 0.0030 g of catalyst. Thus, the optimized reaction conditions for the maximum conversion of benzoin (5 mmol) in MeCN (10 mL) were catalyst (0.0030 g, 5.72 μmol), DMSO (1 mL) and 80 °C. Complexes **1** and **3** as catalysts under the above reaction conditions afforded 50 and 53 % conversion, respectively, in 24 h of reaction time. A blank reaction without catalyst under the above reaction conditions gave only 9 % conversion.

Table 3. OAT between DMSO (1 mL) and benzoin (1.06 g, 5 mmol) with **2** as the catalyst after 24 h of reaction time.

| Entry | Catalyst [g, μmol] | Temperature [°C] | Conversion [%] |
|---|---|---|---|
| 1 | 0.0010, 1.91 | 60 | 16 |
| 2 | 0.0010, 1.91 | 70 | 28 |
| 3 | 0.0010, 1.91 | 80 | 38 |
| 4 | 0.0020, 3.81 | 80 | 73 |
| 5[a] | 0.0030, 5.72 | 80 | 90 |
| 6 | – | 80 | 9 |
| 7[b] | 0.0030, 5.72 | 80 | 0 |

[a] Optimized reaction conditions. [b] The reaction was performed under the optimized conditions but in the absence of DMSO.

The substituents on the phenyl group(s) directly influence the overall oxygen atom transfer reaction. The substituent may affect the oxygen atom transfer in two ways, that is, (1) the electronic effect caused by the *para* substituent and (2) the steric effect caused by the *ortho* substituent. An associative mechanism involving the nucleophilic attack of the substrate, for example, the attack of the P atom of a tertiary phosphine on an empty orbital of one of the oxido groups of the Mo=O* moiety has been suggested.[10,16,20] In such a case, electron-donating substituents on the *cis*-$[Mo^{VI}O_2]^{2+}$ core are expected to decrease the electrophilicity of the oxido ligand and, thus, destabilize the transition state and result in a low reaction rate. On the other hand, bulky substituents at the *ortho* position hinder the approach of the incoming nucleophile and, thereby, reduce the reaction rates. The systems chosen in the present study do not differ much at the electronic level, as all the three complexes possess electron-donating substituents at the *ortho* and *para* positions. However, the presence of *tert*-butyl groups at the *ortho* positions in **1** and **3** influences the reaction rates greatly, as these complexes gave 50 and 53 % conversion, respectively, compared with 90 % conversion for **2** in 24 h of reaction time; therefore, the overall reaction rate (Table 4) as well as the reaction mechanism are mainly sterically controlled.

Table 4. Conversion, turnover frequency (TOF) and selectivity data for OAT between benzoin and DMSO in acetonitrile at 80 °C in 24 h of reaction time catalyzed by *cis*-$[MoO_2]^{2+}$ complexes.

| Entry | Catalyst | Catalyst [g, μmmol] | Selectivity [%] | Conv. [%] | TOF [$h^{-1}$] |
|---|---|---|---|---|---|
| 1 | **1** | 0.0040, 5.72 | 100 | 50 | 24 |
| 2 | **2** | 0.0030, 5.72 | 100 | 90 | 33 |
| 3 | **3** | 0.0035, 5.72 | 100 | 53 | 22 |

Kinetic and mechanistic studies for oxygen atom transfer reaction between DMSO and benzoin in acetonitrile catalyzed by *cis*-$[Mo^{VI}O_2]^{2+}$ have also been carried out and detailed here. The most active compound, **2**, was chosen as the representative catalyst for the kinetic measurements. For this, a solution of **2** (0.0030 g, 5.72 μmol), benzoin (5 mmol) and DMSO (1 mL) in MeCN (10 mL) was maintained at 80 °C. The reaction was performed over a period of 24 h, and the decrease in the concentration of benzoin and the formation of benzil with time were measured periodically by HPLC with a water/acetonitrile/trifluoroacetic acid mixture (60:40:02) as the eluent.

The rate equation [Equation (1)] for the OAT reaction can be derived by considering the integrated rate law. The plots of

the log of the decrease in concentration of benzoin with time obtained for each catalyst are shown in Figure 7. Assuming that the concentration of the catalyst remains largely unaffected (i.e., does not change with time) during the reaction, we can expect the reaction to follow pseudo-first-order kinetics, as is evident from the straight-line plot (Figure 7). Thus, from Equation (2), the resulting pseudo-first-order rate constants (Table 5) are 0.0185, 0.0409 and 0.0186 $h^{-1}$ for **1**–**3**, respectively.

$$\text{Rate} = k_{obs}[\text{Benzoin}]^x[\text{Catalyst}]^y \quad (1)$$

$$\text{Rate} = k_1[\text{Benzoin}] \quad (2)$$

$$\text{where} \quad k_1 = k_{obs}[\text{Catalyst}]^y \quad (3)$$

$$\ln k_1 = \ln k_{obs} + y\ln[\text{Catalyst}] \quad (4)$$

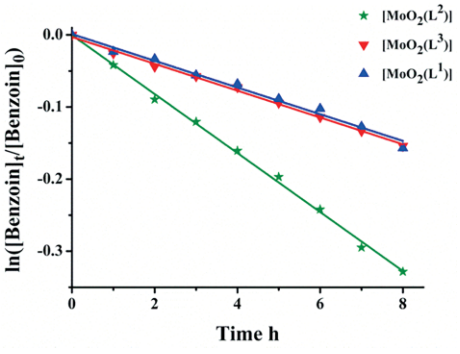


Figure 7. Variation of [benzoin] with time for the OAT reaction in the presence of DMSO catalyzed by **1**–**3**. Reaction conditions: $[\text{benzoin}]_0$ = 5 mmol, DMSO (1.00 mL), catalyst (0.0030 mg) and MeCN (10 mL).

Table 5. Kinetic data for the OAT reaction between benzoin and DMSO in acetonitrile at 80 °C.

| Entry | | $k_1 \pm SE^{[a]}$ [$h^{-1}$] | $k_{obs} \pm SE^{[a]}$ [$M^{-1}$ $h^{-1}$] |
|---|---|---|---|
| 1. | $[MoO_2(L^1)]$ (**1**) | $18.5 \times 10^{-3} \pm 0.74 \times 10^{-3}$ | – |
| 2. | $[MoO_2(L^2)]$ (**2**) | $40.9 \times 10^{-3} \pm 0.72 \times 10^{-3}$ | 0.0162 ± 0.0039 |
| 3. | $[MoO_2(L^3)]$ (**3**) | $18.6 \times 10^{-3} \pm 0.42 \times 10^{-3}$ | – |

[a] SE = standard error.

From the data shown in Figure 7 and rate Equation (4), the order of the reaction with respect to the catalyst concentration can also be derived. Thus, the rate of decrease in the benzoin concentration after 24 h of reaction time at 80 °C in acetonitrile was monitored at different concentrations for the most active catalyst, **2**. The relevant plot (ln $k_1$ vs. ln[catalyst]) is shown in Figure 8; the observed order with respect to catalyst is 0.89, and $k_{obs}$ is 0.0162 $M^{-1}$ $h^{-1}$ (Table 5). Therefore, the overall rate Equation (5) may be represented as shown below.

$$\text{Rate} = k_{obs}[\text{Benzoin}][\text{Catalyst}] \quad (5)$$

$$k_{obs} = 0.0162\ M^{-1}\ h^{-1}$$

The low conversion of 9 % (Table 3, Entry 6) for the blank reaction indicates that a weak oxygen transfer pathway between DMSO and benzoin is operative in the absence of catalyst. However, no conversion of benzoin in the absence of DMSO (Table 3, Entry 7) was obtained even after 24 h of reaction time; therefore, no such pathway exists between the catalyst and benzoin. Thus, during the catalytic reaction, DMSO partially oxidizes benzoin to benzil and is reduced to DMS. This DMS then triggers the catalytic redox reaction in which DMS is

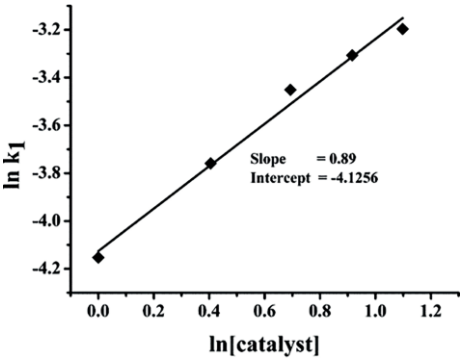


Figure 8. Plot of ln $k_1$ versus ln[catalyst] for the oxotransfer reaction between benzoin and DMSO catalyzed by **2** at 80 °C for 24 h reaction time.

reoxidized back to DMSO by $[Mo^{VI}O_2L]$ to form the $[Mo^{IV}OL]$ species [Equation (6)]; again, DMSO oxidizes benzoin, and the catalytic cycle continues. Accordingly, the oxygen atom transferred to benzoin does not come from the $[Mo^{VI}O_2]$ complex as no reaction is observed in the absence of DMSO, as noted above. The intermediate $[Mo^{IV}OL]$ can then regenerate the original complex $[Mo^{VI}O_2L]$ upon the abstraction of an oxygen atom from the excess DMSO, in a fashion similar to DMSO reductases, and convert it to DMS. Thus, the generation of DMS also increases (see Figure S11) with time along with the formation of benzil.

$$[Mo^{VI}O_2(L^n)] + \text{DMS} \rightleftharpoons [Mo^{IV}O(L^n)] + \text{DMSO} \quad (6)$$

$$[Mo^{VI}O_2(L^n)] + [Mo^{IV}O(L^n)] \rightleftharpoons \overset{O}{\overset{\|}{Mo^{V}}}L^n[-O-\overset{O}{\overset{\|}{Mo^{V}}}L^n] \quad (7)$$

Alternatively, the $[Mo^{IV}OL]$ intermediate can combine with $[Mo^{VI}O_2L]$ to give an intermediate $[LMo^{V}$–μ–O–$Mo^{V}L]$ [Equation (7)]. Here, the order of the reaction with respect to the catalyst concentration offers a suitable explanation for the possible metal complex intermediate(s) involved in the mechanism for OAT reaction. As the obtained order of the reaction with respect to the catalyst concentration is unity, we expect that the dimer formation through $[Mo^{IV}OL]$ is fast and reversible.

Other additional experiments were performed to substantiate this observation. The first evidence was obtained through UV/Vis spectroscopy. The time-dependent UV/Vis spectra for the reaction mixture [i.e., a solution of **2** (0.0030 g), benzoin

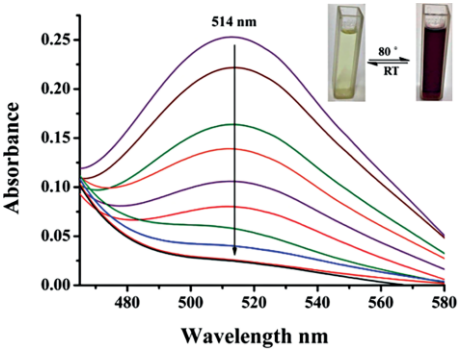


Figure 9. Time-dependent spectral changes observed in the OAT reaction between **2**, benzoin and DMSO in acetonitrile after 6 h of reaction time. The spectra were recorded every 10 s from 80 to ca. 25 °C.

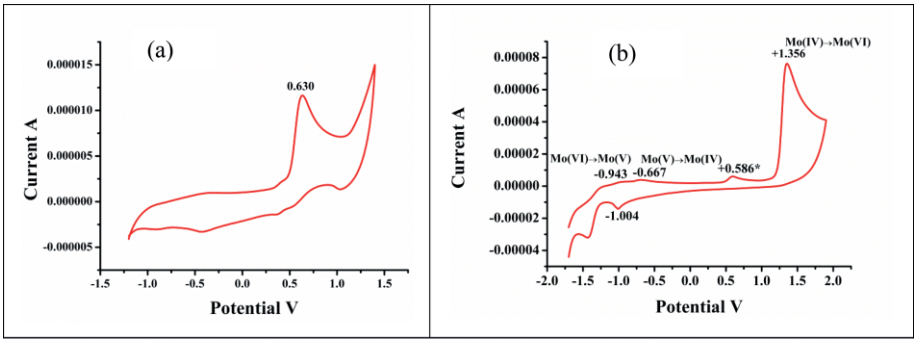


Figure 10. Cyclic voltammograms of (a) $H_2\mathbf{L^2}$ and (b) **2** in MeCN at room temp. (* indicates ligand-centred oxidations).

Table 6. Electrochemical data.

| Compound | First reduction [V] $Mo^{VI}\rightarrow Mo^{V}$ | | | Second reduction [V] $Mo^{V}\rightarrow Mo^{IV}$ | | | First oxidation [V] $Mo^{IV}\rightarrow Mo^{VI}$ | | | $\Delta E_{1/2}$[a] [V] |
|---|---|---|---|---|---|---|---|---|---|---|
| | $E_{pc}$ | $E_{pa}$ | $\Delta E_p$ | $E_{pc}$ | $E_{pa}$ | $\Delta E_p$ | $E_{pc}$ | $E_{pa}$ | $\Delta E_p$ | |
| **1** | –0.817 | –0.776 | 0.041 | 0.519 | 0.476 | 0.043 | 1.396 | – | – | 2.212 |
| **2** | –0.943 | –1.004 | 0.086 | –0.667 | – | – | 1.356 | – | – | 2.299 |
| **3** | –0.776 | –0.724 | 0.052 | –0.642 | –0.463 | 0.179 | 1.367 | – | – | 2.143 |

[a] $\Delta E_{1/2}$ = first oxidation – first reduction.

(5 mmol) and DMSO (1 mL) in MeCN (10 mL)] at 80 °C showed the generation of a broad band at $\lambda \approx 514$ nm, which pinpoints the formation of the oxido-bridged $Mo^{V}$–μ-O–$Mo^{V}$ dimer in solution.[33] This transition is believed to be independent of the nature of the ligand and is assumed to be associated with a charge-transfer transition localized on the $Mo^{V}$–μ-O–$Mo^{V}$ bridge.[34] However, this band decayed quickly and diminished completely in ca. 90 seconds at room temperature (Figure 9). The colour changes of the reaction mixture from yellow to dark purple at high temperature and then back to yellow at room temperature are reproducible and can also be visualized (see inset of Figure 9). The dark purple dinuclear intermediate [$L^2Mo^{V}$–μ-O–$Mo^{V}L^2$] dominates at high temperature in the presence of benzoin and DMSO. However, the original yellow [$Mo^{VI}O_2L$] regenerates on cooling; therefore, the reaction is fast and reversible. Thus, we may propose that the reaction is functional only at high temperature and slow (or no reaction occurs) at low temperature. This is further supported by the following: (1) At lower temperatures (i.e., 60 and 70 °C), the conversions are lower (see Table 3, Entries 1 and 2) than that obtained at 80 °C, which further suggests that the $Mo^{VI}/Mo^{IV}$ redox couple is more active at high temperature, and this is the key to the catalytic process. (2) The order of the reaction with respect to the catalyst concentration is unity for the oxygen atom transfer reaction between benzoin and DMSO catalyzed by *cis*-$[Mo^{VI}O_2]^{2+}$ complexes in acetonitrile (vide supra). (3) All complexes are stable in DMSO, and no electronic spectral changes or colour changes were observed upon heating them in DMSO alone or in a mixture of DMSO and acetonitrile.

The formation of the dinuclear intermediate was further substantiated by the MALDI-TOF mass spectrum of the hot reaction mixture with **2** as the catalyst. A low-intensity peak at $m/z$ = 1058.924 can be attributed to $[(L^2Mo^{V}$–μ-O–$Mo^{V}L^2) + Na + 3H]^+$ (calcd. 1058.977, Figure S12).

Further insights into the reaction pathways were provided by the study of the electrochemical properties of these metal complexes in MeCN. The cyclic voltammograms of $H_2\mathbf{L^2}$ and **2** are presented in Figure 10 (for the other voltammograms, see Figures S13–S15 and Table S2). All three ligands display an irreversible oxidation peak at 0.756, 0.630 and 0.683 V for $H_2\mathbf{L^1}$, $H_2\mathbf{L^2}$ and $H_2\mathbf{L^3}$, respectively. The corresponding complexes **1**, **2** and **3** display two weak reduction couples, the first at –0.812, –0.943 and –0.776 V and the second at –0.519, –0.667 and –0.642 V versus saturated calomel electrode (SCE), respectively, in MeCN. The two reduction couples appears to be reversible for **1** and **3** ($\Delta E_p$ < 59.2 mV), whereas, for **2**, the first reduction potential is quasireversible, and the second reduction is irreversible. However, considering the weak anodic/cathodic currents observed for the reduction potentials, we have classified the reductions as quasireversible in all cases. These are tentatively assigned to $Mo^{VI}/Mo^{V}$ and $Mo^{V}/Mo^{IV}$ reductions. In addition, all three complexes also exhibit an intense oxidation peak at 1.396, 1.356 and 1.367 V for **1**–**3**, respectively, which is attributed to $Mo^{IV}/Mo^{VI}$ oxidations. These values indicate that reduction is slightly easier for **2** than for **1** and **3**. Apparently, this can account for the highest conversion obtained for **2** among the three complexes. A weak oxidation observed at 0.693 and 0.586 V, respectively, for **1** and **2** can be attributed to ligand-centred oxidations; however, it is not very prominent in the voltammogram of **3**. The relevant electrochemical data is presented in Table 6.

## Molybdenum Hydroxylase Activity – Catalytic Oxidation of Pyrogallol

Pyrogallol–phloroglucinol transhydroxylase catalyzes the oxidation of pyrogallol to phloroglucinol anaerobically in the presence of 1,2,3,5-tetrahydroxybenzene as the cosubstrate.[24–26] Recently, it was also shown that the vanadate-dependent peroxidase-like oxidation of pyrogallol gives purpurogallin with a characteristic absorbance at $\lambda$ = 417 nm.[35] We have studied the efficacy of *cis*-$[MoO_2]^{2+}$ to catalyze the oxidation of pyro-

gallol aerobically in the presence of peroxide (Scheme 2). The reaction was initially performed at pH 7 in the presence of $H_2O_2$. This resulted in the generation of a new band characteristic of purpurogallin at $\lambda$ = 417 nm (Figure 11).[35,36] Thus, the reaction appeared to follow the peroxidase pathway. However, the reactivity of **2** with $H_2O_2$ did not indicate the formation of any peroxide intermediate, as no visible spectral or colour changes were observed. Therefore, to get further insights into the reaction mechanism, the reactivity of **2** with pyrogallol was studied in aqueous acetonitrile (1:1). Progressive additions of pyrogallol solution to a solution of **2** in MeCN led to the generation of a new band at $\lambda$ = 267 nm with increasing intensity; however, no band for purpurogallin was observed, and the final spectrum matched that of pure phloroglucinol (Figure 12). The oxidation of pyrogallol by pyrogallol–phloroglucinol hydroxylases proceeds in the presence of 1,2,3,5-tetrahydroxybenzene as the cosubstrate. It has also been established in a few studies that the hydroxy group transferred to pyrogallol does not come from water.[37] Thus, the mechanism followed in the present study appears to be the peroxidase type. However, the possibility of an underlying pyrogallol–phloroglucinol hydroxylase mechanism cannot be ruled out completely. Thus, the exact mechanism for the oxidation of pyrogallol by *cis*-$[MoO_2]^{2+}$ complexes in the present study could not be ascertained unequivocally. Nevertheless, kinetic studies were performed with the assumption that the reaction exhibits peroxidase behaviour.

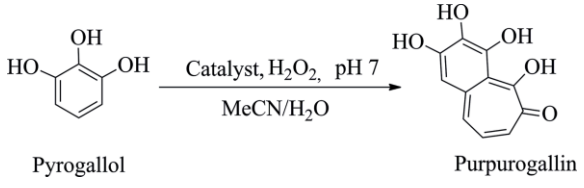


Scheme 2. Oxidation of pyrogallol to purpurogallin via phloroglucinol.

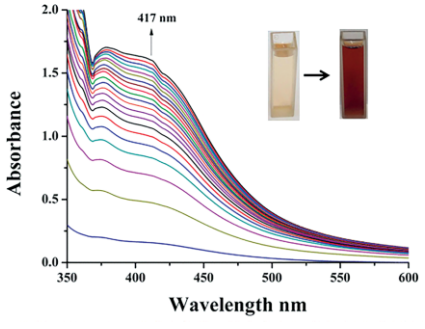


Figure 11. Increment in absorbance at $\lambda$ = 417 nm with time. The spectra were recorded every 3 min. Reaction conditions: pyrogallol (1 mL, $2.5 \times 10^{-2}$ M), phosphate buffer solution (pH 7, 1 M, 1 mL), $H_2O_2$ solution (1 mL, $2.5 \times 10^{-2}$ M) and $[MoO_2(\mathbf{L^2})]$ solution (1 mL, $2.5 \times 10^{-4}$ M).

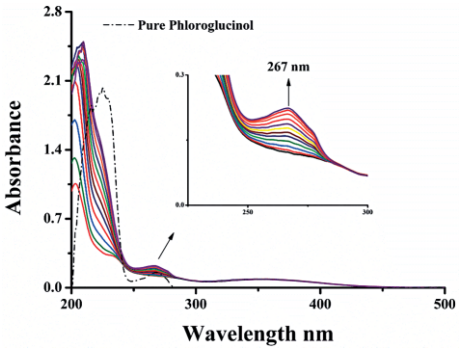


Figure 12. Spectral changes obtained for progressive additions of a pyrogallol solution ($2.5 \times 10^{-3}$ M) to a solution of **2** (10 mL, ca. $1.12 \times 10^{-5}$ M) in MeCN.

The reaction was initiated by the addition of a solution of pyrogallol (1 mL, $2.5 \times 10^{-2}$ M in $H_2O$) to pH 7 phosphate-buffered solution (1 mL, 1 M), followed by the addition of $H_2O_2$ solution (1 mL, $2.5 \times 10^{-2}$ M) and catalyst (1 mL, $2.5 \times 10^{-4}$ M in MeCN). The reaction progress was monitored by checking the increment of the absorbance at $\lambda$ = 417 nm every 3 min for 2 h. As the reaction progressed, the intensity of the band continued to increase. Simultaneously, the reaction mixture slowly turned dark orange owing to the formation of purpurogallin.

The effect of the amount of catalyst on the reaction efficacy was determined with **2** as the representative catalyst. Thus, three different reactions were performed with different dilutions of catalyst solution (i.e., $2.5 \times 10^{-3}$, $2.5 \times 10^{-4}$ and $2.5 \times 10^{-5}$ M, 1 mL of each) in MeCN with the other parameters constant [i.e., 1 mL each of pyrogallol ($2.5 \times 10^{-2}$ M), aqueous $H_2O_2$ ($2.5 \times 10^{-2}$ M), pH 7 phosphate buffer (1 M) in $H_2O$]. The corresponding spectra obtained after 2 h of reaction time are shown in Figure 13. It is evident that $2.5 \times 10^{-4}$ M catalyst gave the same results as $2.5 \times 10^{-3}$ M catalyst, whereas poor results were

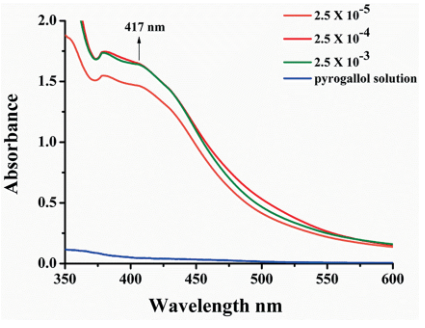


Figure 13. Final spectra of different reaction mixtures obtained after 2 h containing different concentration of the catalyst solution, pyrogallol solution ($2.5 \times 10^{-2}$ M, 1 mL) and $H_2O_2$ solution ($2.5 \times 10^{-2}$ M, 1 mL). The spectrum of pure pyrogallol solution is also included. For experimental details, see text.

Table 7. Kinetic parameters for the oxidation of pyrogallol by $[MoO_2(\mathbf{L^{1-3}})]$.

| Entry | Compound | $V_{max} \pm SE$[a] [μM $s^{-1}$] | $K_M \pm SE$[a] [mM] | $k_{cat} \pm SE$[a] [$h^{-1}$] |
|---|---|---|---|---|
| 1 | **1** | 0.7975 ± 0.0556 | 12.47 ± 1.5 | 394 ± 5.24 |
| 2 | **2** | 0.6070 ± 0.0219 | 11.85 ± 1.3 | 300 ± 6.35 |
| 3 | **3** | 0.4623 ± 0.0539 | 7.06 ± 1.7 | 247 ± 5.43 |

[a] SE = standard error.

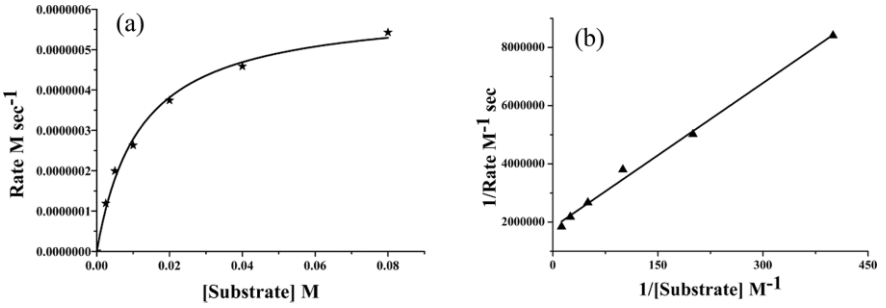


Figure 14. (a) Michaelis–Menten and (b) Lineweaver–Burk plots for **2**.

obtained with $2.5 \times 10^{-5}$ M catalyst. Thus 1 mL of $2.5 \times 10^{-4}$ M catalyst for 1 mL of $2.5 \times 10^{-2}$ M pyrogallol was considered ideal for catalytic activity. The full spectral changes observed with time for 1 mL each of $2.5 \times 10^{-4}$ M [$MoO_2(L^2)$] (**2**) as catalyst, $2.5 \times 10^{-2}$ M pyrogallol, $2.5 \times 10^{-2}$ M $H_2O_2$ and 1 M phosphate buffer of pH 7 are shown in Figure 11. For similar results with complexes **1** and **3** as catalysts, see Figures S16 and S17.

To evaluate the peroxidase mimetic activity of complexes **1**–**3**, steady-state kinetic studies were performed in MeCN at pH 7, and the kinetic parameters, $V_{max}$, $K_M$ and $k_{cat}$ were determined with Michaelis–Menten behaviour assumed for the system (Table 7). The Michaelis–Menten equation for a single substrate reaction may be expressed as

$$V_i = V_{max} \times \frac{[S]}{K_M + [S]}$$

$V_i$ is the initial reaction velocity and [S] is the substrate concentration.

Different concentrations of pyrogallol solution (0.00250–0.0800 M) were added to $2.5 \times 10^{-5}$ M solutions of **1**–**3** in phosphate buffer (1 M, 1 mL) and $H_2O_2$ ($2.5 \times 10^{-3}$ M, 1 mL). For each substrate–complex mixture, the spectra were recorded for a period of 3 min immediately after preparation of the pyrogallol solution. The initial rates were obtained from the linear regression of absorbance versus time plots. The initial rates and the substrate concentrations were then fitted to the Michaelis–Menten equation through nonlinear regression analysis with the Origin 8.0 software.

Initially, at low substrate concentrations, the reaction follows first-order kinetics. As frequently encountered in enzyme kinetics, increasing the substrate concentration eventually saturates the enzyme sites, and the reaction becomes zero order and independent of substrate concentration (Figure 14 for **2** as a representative and Figures S18 and S19 for the others). Thus, we may conclude that the present *cis*-$[MoO_2]^{2+}$ complexes follow Michaelis–Menten-type kinetics with respect to pyrogallol. The various kinetic parameters obtained for each of the enzyme mimics are presented in Table 7.

## Conclusions

Three dibasic tetradentate tripodal Mannich bases $H_2L^1$, $H_2L^2$, and $H_2L^3$ derived from aminoethylmorpholine and 2,4-disubstituted phenols were prepared in good yields. These ligands were used to prepare the corresponding *cis*-dioxidomolybdenum complexes [$MoO_2(L^1)$] (**1**), [$MoO_2(L^2)$] (**2**) and [$MoO_2(L^3)$] (**3**) through 1:1 molar reactions in methanol. The prepared complexes were employed successfully as catalysts for oxygen atom transfer in a fashion similar to DMSO reductase. The reaction was performed between benzoin and DMSO at 80 °C in acetonitrile as the solvent. The reactions were monitored by HPLC analysis, and the best conversion of 90 % was achieved after a period of 24 h. A detailed kinetic study revealed that the reaction is first order in both the catalyst and the substrate, and the second-order rate constant is 0.0162 $M^{-1}$ $h^{-1}$. A possible mechanistic pathway and the intermediates involved were also evaluated, and the formation of the dinuclear intermediate [$LMo^V$–μ-O–$Mo^V$L] and its fast decay to the initial monomeric form were confirmed through UV/Vis spectroscopy and MALDI MS studies of the reaction mixture. The *cis*-dioxidomolybdenum complexes were also engaged in the catalytic oxidation of pyrogallol, a process thought to mimic the activity of peroxidases. The initial oxidation product, phloroglucinol, underwent further oxidative coupling to give purpurogallin as the final product in the presence of $H_2O_2$. The reaction was shown to follow Michaelis–Menten-type kinetics with respect to pyrogallol. The turnover numbers for the three catalysts **1**–**3** are 394, 300 and 247 $h^{-1}$, respectively.

## Experimental Section

**Materials and General Methods:** Ammonium molybdate, acetylacetone, pyrogallol (Loba Chemie, India), 2,4-di-*tert*-butylphenol (Himedia, India), 2,4-dimethylphenol, 2-*tert*-butyl-4-methylphenol, aminoethylmorpholine (Aldrich, USA), 30 % aqueous $H_2O_2$ (Qualigens, India), benzoin (S. D. fine chemicals, India), formaldehyde and DMSO (Rankem, India) were used as obtained. Other chemicals and solvents were of AR grade. The precursor complex [$Mo^{VI}O_2(acac)_2$] was prepared by a literature method.[38]

All measurements were made after the metal complexes were dried at 100 °C. Elemental analyses of the complexes were performed with an Elementar model Vario-EI-III analyzer after the samples were dried at 100 °C. The IR spectra of samples as KBr pellets were recorded with a Nicolet 1100 FTIR spectrometer. The electronic spectra of the complexes in acetonitrile were recorded with a Shimadzu 1601 UV/Vis spectrophotometer. The $^1H$ and $^{13}C$ NMR spectra were recorded with a JEOL ECX 400 MHz spectrometer with samples in [$D_6$]DMSO for the $^1H$ NMR spectra and in $CDCl_3$ for the $^{13}C$ NMR spectra of the ligands. We attempted to obtain the $^{13}C$ NMR spectra of the complexes in $CD_3CN$, [$D_6$]DMSO and [$D_6$]benzene but did not observe satisfactory signals even after 4000 scans. The thermogravi-

metric analyses of the complexes were performed with a Perkin–Elmer (Pyris Diamond) instrument in air with a heating rate of 10 °C min$^{-1}$. GC–MS was performed with a Perkin–Elmer Clarus 500 instrument. The PXRD data were collected with a Bruker Advanced D8 diffractometer with Cu-$K_\alpha$ radiation in the $2\theta$ range 5–50° at a scan speed of 0.2° min$^{-1}$. The MALDI-TOF mass spectra were measured with a Bruker Ultra-fleXtreme-TN MALDI-TOF/TOF spectrometer with 2-(4′-hydroxybenzeneazo)benzoic acid (HABA) as the matrix. The electrochemical measurements were performed with a CH Instruments electrochemical workstation instrument with a Pt working electrode, a standard calomel electrode as the reference electrode and a Pt wire counter electrode in acetonitrile solutions under an argon atmosphere. The supporting electrolyte was 0.1 M $Bu_4NPF_6$ (Fluka), which was recrystallized twice with ethanol before use. The measurements were calibrated to ferrocene as an external standard. The ferrocene/ferrocenium couple was found at $E_{1/2}$ = +0.39 V versus SCE under the employed experimental conditions. HPLC-grade acetonitrile for electrochemistry was dried with molecular sieves (pore size 4 Å). HPLC was performed with a Shimadzu LC-2010A HT instrument in low-pressure gradient mode with a flow rate of 0.5 mL min$^{-1}$ and an injection volume of 15 µL. The mobile phase was MeCN/$H_2O$/trifluoroacetic acid (60:40:0.02).

**X-ray Crystal-Structure Determination:** Three-dimensional X-ray data were collected with a Bruker Kappa Apex CCD diffractometer at room temperature for **1**, **2** and **3** by the $\phi$–$\omega$ scan method. Reflections were measured from a hemisphere of data collected from frames, each covering 0.3° in $\omega$. Totals of 66929, 17142 and 20467 reflections were measured for **1**–**3**, respectively, and corrected for Lorentz and polarization effects and for absorption by multiscan methods based on symmetry-equivalent and repeated reflections. Of the total, 4362, 4203 and 4631 independent reflections for **1**–**3**, respectively, exceeded the significance level ($|F|/\sigma|F|$) > 4.0. After data collection, an empirical absorption correction (SADABS)[39] was applied, and the structures were solved by direct methods and refined by full-matrix least-squares on $F^2$ data with the SHELX suite of programs.[40] The hydrogen atoms were included in calculated positions and refined with a riding mode. The refinements were performed with allowance for the thermal anisotropy of all non-hydrogen atoms. The crystal of **3** presented significant disorder of the methyl groups around the tripodal nitrogen atom. The disorder of the methyl groups was resolved, and the atomic sites were observed and refined with anisotropic atomic displacement parameters. The site occupancy factor was 0.56563 for C(6A), C(7A) and C(19A). A final difference Fourier map showed no residual density outside 0.967 and –0.820 e Å$^{-3}$ for **1** and 0.668 and –0.403 e Å$^{-3}$ for **2**. In **3**, a final difference Fourier map showed high residual density outside 1.051 and –1.506 e Å$^{-3}$ owing to the disorder of the carbon atoms. Weighting schemes $w = 1/[\sigma^2(F_o^2) + (0.122000P)^2 + 0.00000P]$ for **1**, $w = 1/[\sigma^2(F_o^2) + (0.041100P)^2 + 0.532700P]$ for **2** and $w = 1/[\sigma^2(F_o^2) + (0.086000P)^2 + 3.613500P]$ for **3**, in which $P = (|F_o|^2 + 2|F_c|^2)/3$, were used in the latter stages of the refinements. Further details of the crystal-structure determination are given in Table 8.

CCDC 1473616 (for **1**), 1473617 (for **2**) and 1473618 (for **3**) contain the supplementary crystallographic data for this paper. These data can be obtained free of charge from The Cambridge Crystallographic Data Centre.

**$H_2L^1$:** A solution of aminoethylmorpholine (0.651 g, 5 mmol), formaldehyde (39 %, 0.770 g, 10 mmol) and 2,4-di-*tert*-butylphenol (2.063 g, 10 mmol) in MeOH (20 mL) was heated under reflux for ca. 18 h. During this period, a white solid separated slowly; the solid was collected by filtration, washed well with cold MeOH and recrystallized from ethanol, yield 4.1 g (73 %). $C_{36}H_{58}N_2O_3$ (566.86): calcd. C 76.28, H 10.31, N 4.94; found C 76.19, H 10.15, N 4.90. IR: $\tilde{\nu}_{max}$ = 3184 (OH), 2954, 2899, 2867 (*tert*-butyl), 1481, 1445, 1361, 1221, 1147, 1118, 877, 862, 770, 610, 580 cm$^{-1}$. $^1$H NMR ([D$_6$]DMSO): $\delta$ = 9.637 (s, 2 H, –OH), 7.115–7.110 (d, 2 H, Ar), 6.958–6.953 (d, 2 H, Ar), 3.757–3.735 (t, 4 H, $NCH_2CH_2$), 3.569 (s, 4 H, $NCH_2Ar$), 2.683–2.654 (m, 2 H, morpholine ring), 2.542–2.516 (m, 4 H, morpholine ring), 2.468–2.424 (m, 2 H, morpholine ring), 1.326 [s, 18 H, $-C(CH_3)_3$], 1.221 [s, 18 H, $-C(CH_3)_3$] ppm. $^{13}$C NMR ($CDCl_3$): $\delta$ =

Table 8. Crystal data and structure refinement for **1**–**3**.

| | **1** | **2** | **3** |
|---|---|---|---|
| Formula | $C_{37}H_{60}MoN_2O_6$ | $C_{24}H_{32}MoN_2O_5$ | $C_{30}H_{44}MoN_2O_5$ |
| Formula weight | 724.81 | 524.46 | 608.61 |
| $T$ [K] | 293(2) | 293(2) | 293(2) |
| Wavelength [Å] | 0.71073 | 0.71073 | 0.71073 |
| Crystal system | monoclinic | triclinic | monoclinic |
| Space group | *C*2/*c* | $P\bar{1}$ | *C*2/*c* |
| $a$ [Å] | 27.0086(11) | 8.3103(3) | 31.578(2) |
| $b$ [Å] | 11.4464(5) | 10.2983(4) | 7.4650(6) |
| $c$ [Å] | 27.1802(12) | 14.8691(5) | 27.551(2) |
| $\alpha$ [°] | 90 | 70.816(2) | 90 |
| $\beta$ [°] | 114.047(3) | 73.912(2) | 113.046(4) |
| $\gamma$ [°] | 90 | 84.022(2) | 90 |
| $V$ [Å$^3$] | 7673.5(6) | 1154.67(7) | 5976.3(8) |
| Z | 8 | 2 | 8 |
| $F$(000) | 3088 | 544 | 2560 |
| $D_{calcd}$ [g cm$^{-3}$] | 1.255 | 1.508 | 1.353 |
| $\mu$ [mm$^{-1}$] | 0.385 | 0.606 | 0.478 |
| $\theta$ [°] | 1.64 to 28.29 | 1.50 to 28.33 | 1.40 to 28.38 |
| $R_{int}$ | 0.1595 | 0.0474 | 0.0594 |
| Crystal size [mm] | 0.29 × 0.24 × 0.21 | 0.22 × 0.21 × 0.18 | 0.21 × 0.18 × 0.16 |
| Goodness-of-fit on $F^2$ | 0.984 | 1.013 | 1.068 |
| $R_1$ [$I > 2\sigma(I)$][a] | 0.0787 | 0.0433 | 0.0599 |
| $wR_2$ (all data)[b] | 0.2447 | 0.1023 | 0.1783 |
| Largest difference peak and hole [e Å$^{-3}$] | 0.967 and –0.820 | 0.668 and –0.403 | 1.051 and –1.506 |

[a] $R_1 = \Sigma||F_o| - |F_c||/\Sigma|F_o|$. [b] $wR_2 = \{\Sigma[w(||F_o|^2 - |F_c|^2|)^2]/\Sigma[w(F_o^2)^2]\}^{1/2}$.

152.81, 140.69, 136.03, 124.97, 123.61, 121.25, 66.07, 56.26, 54.99, 53.65, 48.03, 35.04, 34.18, 31.77, 29.63 ppm.

**$H_2L^2$ and $H_2L^3$:** These ligands were prepared in 63 and 71 % yields, respectively, by the procedure outlined for $H_2L^1$ by using 2,4-dimethylphenol (1.221 g, 10 mmol) or 2-*tert*-butyl-4-methylphenol (1.642 g, 10 mmol) in place of 2,4-di-*tert*-butylphenol.

**Data for $H_2L^2$:** $C_{24}H_{34}N_2O_3$ (398.538): calcd. C 72.33, H 8.60, N 7.03; found C 72.13, H 8.52, N 7.12. IR: $\tilde{\nu}_{max}$ = 3155 (–OH), 2958, 2913, 2861 (alkyl), 1486, 1377, 1308, 1283, 1218, 1115, 1071, 862, 768, 741, 618, 580 $cm^{-1}$. $^1H$ NMR ([D$_6$]DMSO): $\delta$ = 9.203 (s, 2 H, –OH), 6.807–6.802 (d, 2 H, Ar), 6.727–6.724 (d, 2 H, Ar), 3.655–3.632 (t, 4 H, $NCH_2CH_2$), 3.326 (s, 4 H, $NCH_2Ar$), 2.570–2.540 (m, 2 H, morpholine ring), 2.483–2.454 (m, 2 H, morpholine ring), 2.293–2.264 (m, 2 H, morpholine ring), 2.136 (s, 6 H, $CH_3$), 2.077 (s, 6 H, $CH_3$) ppm. $^{13}C$ NMR ($CDCl_3$): $\delta$ = 152.16, 131.35, 128.44, 127.80, 125.49, 121.54, 60.09, 55.65, 54.99, 53.63, 47.95, 20.47, 16.03 ppm.

**Data for $H_2L^3$:** $C_{30}H_{46}N_2O_3$ (482.69): calcd. C 74.65, H 9.61, N 5.80; found C 74.54, H 9.52, N 5.82. IR: $\tilde{\nu}_{max}$ = 3190 (–OH), 2872, 2910, 2953 (alkyl), 1478, 1445, 1356, 1286, 1231, 1180, 1118, 1023, 862, 812, 773, 548, 519, 502 $cm^{-1}$. $^1H$ NMR ([D$_6$]DMSO): $\delta$ = 9.451 (s, 2 H, –OH), 6.900–6.894 (d, 2 H, Ar), 6.779–6.763 (d, 2 H, Ar), 3.744–3.717 (t, 4 H, $NCH_2CH_2$), 3.506 (s, 4 H, $NCH_2Ar$), 3.341–3.324 (m, 4 H, morpholine ring), 2.675–2.645 (m, 2 H, morpholine ring), 2.439–2.318 (m, 2 H, morpholine ring), 2.168 (s, 6 H, $CH_3$), 1.130 [s, 18 H, $–C(CH_3)_3$] ppm. $^{13}C$ NMR ($CDCl_3$): $\delta$ = 152.90, 136.76, 128.87, 127.34, 127.22, 122.09, 66.07, 55.76, 54.89, 53.48, 47.98, 34.72, 29.58, 20.83 ppm.

Further details of the $^{13}C$ NMR spectroscopic data and assignments of important signals are given in Table S2.

**[$Mo^{VI}O_2(L^1)$] (1):** To a suspension of $H_2L^1$ in MeOH (0.567 g, 1 mmol, 10 mL) was added a filtered solution of [$Mo^{VI}O_2(acac)_2$] (0.326 g, 1 mmol) in MeOH (10 mL) with stirring to afford a clear orange solution after ca. 15 min. The orange solution was then heated under reflux for 3 h with a hot water bath. The yellow solid that separated as the reaction mixture cooled to room temperature was collected by filtration, washed with cold MeOH and dried under vacuum, yield 0.485 g (70 %). $C_{36}H_{56}MoN_2O_5$ (692.80): calcd. C 62.41, H 8.15, N 4.04; found C 61.85, H 7.98, N 4.01. Crystals of **1** suitable for X-ray diffraction were grown through the slow evaporation of a MeOH solution at room temperature. IR: $\tilde{\nu}_{max}$ = 2954, 2903, 2866 (*tert*-butyl), 1467, 1442, 1361, 1240, 1204, 1170, 1119, 933 $(MoO_2)_{asym}$, 906 $(MoO_2)_{sym}$, 843, 753, 600, 555, 496 $cm^{-1}$. $^1H$ NMR ([D$_6$]DMSO): $\delta$ = 7.175–7.170 (d, 2 H, Ar), 7.080–7.069 (d, 2 H, Ar), 4.159–4.122 (d, $J$ = 14.8 Hz, 2 H, $NCH_2Ar$), 4.043–4.005 (d, $J$ = 15.2 Hz, 2 H, $NCH_2Ar$), 3.912–3.880 (t, 2 H, $NCH_2CH_2$), 3.826–3.774 (t, 2 H, $NCH_2CH_2$), 3.735–3.680 (m, 2 H, morpholine ring), 2.980–2.948 (m, 2 H, morpholine ring), 2.768–2.738 (m, 2 H, morpholine ring), 2.070–2.069 (m, 2 H, morpholine ring), 1.353 [s, 18 H, $–C(CH_3)_3$], 1.251 [s, 18 H, $–C(CH_3)_3$] ppm.

**[$Mo^{VI}O_2(L^2)$] (2):** This complex was prepared similarly to **1** with $H_2L^2$ (0.399 g, 1 mmol) instead of $H_2L^1$, yield 0.398 g (76 %). $C_{24}H_{32}MoN_2O_5$ (524.46): calcd. C 54.96, H 6.15, N 5.34; found C 54.58, H 6.25, N 5.26. Crystals of **2** suitable for X-ray diffraction were grown through the slow evaporation of a DMSO solution at room temperature. IR: $\tilde{\nu}_{max}$ = 2961, 2919, 2878 (alkyl), 1464, 1310, 1248, 1214, 1142, 1113, 918 $(MoO_2)_{asym}$, 870 $(MoO_2)_{sym}$, 834, 762, 750, 585, 552, 515 $cm^{-1}$. $^1H$ NMR ([D$_6$]DMSO): $\delta$ = 6.939–6.935 (d, 2 H, Ar), 6.843–6.838 (d, 2 H, Ar), 4.368–4.332 (d, $J$ = 14.4 Hz, 2 H, $NCH_2Ar$), 3.909–3.873 (d, $J$ = 14.4 Hz, 2 H, $NCH_2Ar$), 4.169–4.116 (t, 2 H, $NCH_2CH_2$), 3.743–3.703 (t, 2 H, $NCH_2CH_2$), 3.185–3.163 (m, 2 H, morpholine ring), 2.670–2.600 (m, 4 H, morpholine ring), 2.471–2.453 (m, 2 H, morpholine ring), 2.202 (s, 6 H, $CH_3$), 2.067 (s, 6 H, $CH_3$) ppm.

**[$Mo^{VI}O_2(L^3)$] (3):** Complex **3** was prepared similarly to **1** with $H_2L^3$ instead of $H_2L^1$ (0.483 g, 1 mmol), yield 0.401 g (66 %). $C_{30}H_{44}MoN_2O_5$ (608.64): calcd. C 59.20, H 7.29, N 4.60; found C 59.11, H 6.88, N 4.48. Crystals of **3** suitable for X-ray diffraction were grown through the slow evaporation of a MeCN solution at room temperature. IR: $\tilde{\nu}_{max}$ = 2868, 2915, 2956 (alkyl), 1462, 1442, 1306, 1243, 1229, 1149, 1116, 923 $(MoO_2)_{asym}$, 901 $(MoO_2)_{sym}$, 863, 820, 756, 598, 569, 552 $cm^{-1}$. $^1H$ NMR ([D$_6$]DMSO): $\delta$ = 6.957–6.953 (d, 2 H, Ar), 6.872–6.869 (d, 2 H, Ar), 4.091–4.056 (d, $J$ = 14.0 Hz, 2 H, $NCH_2Ar$), 3.998–3.965 (d, $J$ = 13.2 Hz, 2 H, $NCH_2Ar$), 3.830–3.774 (t, 2 H, $NCH_2CH_2$), 3.722–3.667 (t, 2 H, $NCH_2CH_2$), 3.910–3.878 (m, 2 H, morpholine ring), 3.318–3.316 (m, 2 H, morpholine ring), 2.961–2.932 (m, 2 H, morpholine ring), 2.741–2.711 (m, 2 H, morpholine ring), 2.218 (s, 6 H, $CH_3$), 1.332 [s, 18 H, $–C(CH_3)_3$] ppm.

**Oxotransfer Activity:** A solution of benzoin (1.06 g, 5 mmol), catalyst (0.0030 g, 5.72 μmol) and DMSO (1 mL) in acetonitrile (10 mL) was maintained at 80 °C for 24 h. The progress of the reaction was monitored by HPLC with MeCN/$H_2O$/TFA mixtures (60:40:0.02).

**Molybdenum Hydroxylase Activity – Catalytic Oxidation of Pyrogallol:** The molybdenum hydroxylase activities of all *cis*-$[MoO_2]^{2+}$ complexes were determined at pH 7 in acetonitrile. The reactions were followed by UV/Vis spectroscopy by monitoring the absorbance increment at $\lambda$ = 417 nm owing to the formation of the oxidized product, purpurogallin. The reaction was initiated by the addition of a solution of pyrogallol (1 mL, $2.5 \times 10^{-2}$ M) to phosphate buffer solution (pH 7, 1 M, 1 mL), followed by the addition of $H_2O_2$ solution (1 mL, $2.5 \times 10^{-2}$ M) and the catalyst solution (1 mL, $2.5 \times 10^{-4}$ M). The UV/Vis spectra of the resulting solutions were then recorded every 3 min in repeat scan mode for 2 h. The steady-state kinetics was determined similarly over 3 min, and the initial rates were calculated from the slopes of the absorbance versus time plots. The initial reaction rates were then fitted to the Michaelis–Menten equation and Lineweaver–Burk plots to calculate the maximal velocity ($V_{max}$), Michaelis constant ($K_M$) and catalytic constant or turnover number ($k_{cat}$) from the nonlinear curve with the Origin 8.0 software.

## Acknowledgments

M. R. M. thanks the Science and Engineering Research Board (SERB), Government of India, New Delhi for financial support of the work (grant number EMR/2014/000529). B. U. is thankful to the Indian Institute of Technology (IIT) Roorkee for an MHRD fellowship.

**Keywords:** Molybdenum · Tripodal ligands · Oxido ligands · Oxidation · Kinetics

[1] K. Heinze, *Coord. Chem. Rev.* **2015**, *300*, 121–141.
[2] R. Hille, J. Hall, P. Basu, *Chem. Rev.* **2014**, *114*, 3963–4038.
[3] R. Mayilmurugan, B. N. Harum, M. Volpe, A. F. Sax, M. Palaniandavar, N. C. Mösch-Zanetti, *Chem. Eur. J.* **2011**, *17*, 704–713.
[4] P. Basu, B. W. Kail, A. K. Adams, V. N. Nemykin, *Dalton Trans.* **2013**, *42*, 3071–3081.
[5] D. C. Rees, Y. Hu, C. Kisker, H. Schindelin, *J. Chem. Soc., Dalton Trans.* **1997**, 3909–3914.
[6] A. Majumdar, *Dalton Trans.* **2014**, *43*, 8990–9003.
[7] A. S. McAlpine, A. G. McEwan, S. Bailey, *J. Mol. Biol.* **1998**, *275*, 613–623.
[8] R. Hille, *Chem. Rev.* **1996**, *96*, 2757–2816.

[9] H. Sugimoto, M. Sato, K. Asano, T. Suzuki, K. Mieda, T. Ogura, T. Matsumoto, L. J. Giles, A. Pokhrel, M. L. Kirk, S. Itoh, *Inorg. Chem.* **2016**, *55*, 1542–1550.
[10] J. H. Enemark, J. J. A. Cooney, J.-J. Wang, R. H. Holm, *Chem. Rev.* **2004**, *104*, 1175–1200.
[11] P. V. Bernhardt, *Chem. Commun.* **2011**, *47*, 1663–1673.
[12] M. J. Pushie, G. N. George, *Coord. Chem. Rev.* **2011**, *255*, 1055–1084.
[13] M. J. Pushie, J. J. Cotelesage, G. N. George, *Metallomics* **2014**, *6*, 15–24.
[14] C. J. Whiteoak, G. J. P. Britovsek, V. C. Gibson, A. J. P. White, *Dalton Trans.* **2009**, 2337–2344.
[15] X. Ma, C. Schulzke, H. G. Schmidt, M. Noltemeyer, *Dalton Trans.* **2007**, 1773–1780.
[16] G. Lyashenko, G. Saischek, M. E. Judmaier, M. Volpe, J. Baumgartner, F. Belaj, V. Jancik, R. H. Irmerd, N. C. Mösch-Zanetti, *Dalton Trans.* **2009**, 5655–5665.
[17] R. Dinda, P. Sengupta, S. Ghosh, W. S. Sheldrick, *Eur. J. Inorg. Chem.* **2003**, 363–369.
[18] A. Ducrot, B. Scattergood, B. Coulson, R. N. Perutz, A. K. Duhme-Klair, *Eur. J. Inorg. Chem.* **2015**, 3562–3571.
[19] M. E. Judmaier, A. Wallner, G. N. Stipicic, K. Kirchner, J. Baumgartner, F. Belaj, N. C. Mösch-Zanetti, *Inorg. Chem.* **2009**, *48*, 10211–10221.
[20] P. Basu, B. W. Kail, C. G. Young, *Inorg. Chem.* **2010**, *49*, 4895–4900.
[21] X. Ma, C. Schulzke, Z. Yang, A. Ringe, J. Magull, *Polyhedron* **2007**, *26*, 5497–5505.
[22] C. E. A. Andrade, X. Ma, W. Meyer-Klaucke, C. Schulzke, *Polyhedron* **2010**, *29*, 664–668.
[23] T. Paul, P. M. Rodehutskors, J. Schmidt, N. Burzlaff, *Eur. J. Inorg. Chem.* **2016**, 2595–2602.
[24] C. Kisker, H. Schindelin, D. Baas, J. Reètey, R. U. Meckenstock, P. M. H. Kroneck, *FEMS Microbiol. Rev.* **1999**, *22*, 503–521.
[25] R. Hille, J. Reètey, U. Bartlewski-Hof, W. Reichenbecher, B. Schink, *FEMS Microbiol. Rev.* **1999**, *22*, 489–501.
[26] H. Dobbek, *Coord. Chem. Rev.* **2011**, *255*, 1104–1116.
[27] a) M. R. Maurya, L. Rana, F. Avecilla, *Inorg. Chim. Acta* **2015**, *429*, 138–147; b) M. R. Maurya, N. Saini, F. Avecilla, *RSC Adv.* **2015**, *5*, 101076–101088; c) M. R. Maurya, S. Dhaka, F. Avecilla, *New J. Chem.* **2015**, *39*, 2130–2139; d) M. R. Maurya, S. Dhaka, F. Avecilla, *Polyhedron* **2015**, *96*, 79–87.
[28] Y. L. Wong, Y. Yan, E. S. H. Chan, Q. Yang, T. C. W. Mak, D. K. P. Ng, *J. Chem. Soc., Dalton Trans.* **1998**, 3057–3064.
[29] Y. L. Wong, Q. Yang, Z. Y. Zhou, H. K. Lee, T. C. W. Mak, D. K. P. Ng, *New J. Chem.* **2001**, *25*, 353–357.
[30] A. Lehtonen, R. Sillanpää, *Polyhedron* **2005**, *24*, 257–265.
[31] a) N. K. Ngan, K. M. Lo, C. S. R. Wong, *Polyhedron* **2011**, *30*, 2922–2932; b) F. Madeira, S. Barroso, S. Namorado, P. M. Reis, B. Royo, A. M. Martins, *Inorg. Chim. Acta* **2012**, *383*, 152–156; c) A. Lehtonen, M. Wasberg, R. Sillanpää, *Polyhedron* **2006**, *25*, 767–775; d) R. D. R. S. Manian, R. Leino, O. Wichmann, A. Lehtonen, *Inorg. Chem. Commun.* **2009**, *12*, 1004–1006; e) T. Fang, H. X. Lu, J. X. Zhao, S. Z. Zhan, *Inorg. Chem. Commun.* **2015**, *51*, 66–70; f) J. P. Cao, J. X. Zhao, H. X. Lu, S. Z. Zhan, *Transit. Met. Chem.* **2014**, *39*, 933–937; g) X. Lei, N. Chelamalla, *Acta Crystallogr., Sect. E* **2011**, *67*, m1510; h) C. J. Hinshaw, G. Peng, R. Singh, J. T. Spence, J. H. Enemark, M. Bruck, J. Kristofiski, S. L. Merbs, R. B. Ortega, P. A. Wexler, *Inorg. Chem.* **1989**, *28*, 4483–4491; i) J. W. Lim, Y. C. Park, M. Mikuriya, *Bull. Chem. Soc. Jpn.* **2002**, *75*, 2011–2012.
[32] a) M. R. Maurya, B. Uprety, F. Avecilla, P. Adão, J. Costa Pessoa, *Dalton Trans.* **2015**, *44*, 17736–17755; b) S. K. Kurapati, S. Maloth, S. Pal, *Inorg. Chim. Acta* **2015**, *430*, 66–73; c) X. Lei, N. Chelamalla, *Polyhedron* **2013**, *49*, 244–251; d) T. Heikkilä, R. Sillanpää, A. Lehtonen, *J. Coord. Chem.* **2014**, *67*, 1863–1872; e) Y. L. Wong, L. H. Tong, J. R. Dilworth, D. K. P. Ng, H. K. Lee, *Dalton Trans.* **2010**, *39*, 4602–4611; f) F. Wolff, C. Lorber, R. Choukroun, B. Donnadieu, *Inorg. Chem.* **2003**, *42*, 7839–7845.
[33] J. A. Craig, E. W. Harlan, B. S. Snyder, M. A. Whitener, R. H. Holm, *Inorg. Chem.* **1989**, *28*, 2082–2091.
[34] J. Topich, J. T. Lyon, *Inorg. Chem.* **1984**, *23*, 3202–3206.
[35] a) M. R. Maurya, N. Chaudhary, F. Avecilla, I. Correia, *J. Inorg. Biochem.* **2015**, *147*, 181–192; b) M. R. Maurya, N. Kumar, N. Chaudhary, *Polyhedron* **2015**, *97*, 103–111.
[36] P. C. Pandey, A. K. Pandey, *Electrochim. Acta* **2013**, *109*, 536–545.
[37] a) W. Reichenbecher, B. Schink, *Biochim. Biophys. Acta* **1999**, *1430*, 245–253; b) C. Paizs, U. Bartlewski-Hof, J. Rétey, *Chem. Eur. J.* **2007**, *13*, 2805–2811; c) A. Messerschmidt, H. Niessen, D. Abt, O. Einsle, B. Schink, P. M. H. Kroneck, *Proc. Natl. Acad. Sci. USA* **2004**, *101*, 11571–11576.
[38] G. J. J. Chen, J. W. McDonald, W. E. Newton, *Inorg. Chem.* **1976**, *15*, 2612–2615.
[39] G. M. Sheldrick, *SADABS*, version 2.10, University of Göttingen, Germany, **2004**.
[40] G. M. Sheldrick, *Acta Crystallogr., Sect. A* **2008**, *64*, 112–122.

Received: June 10, 2016
Published Online: ■

 

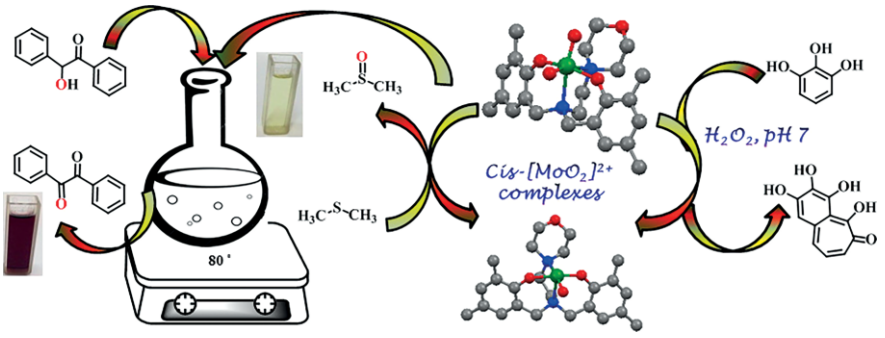


Dioxidomolybdenum(VI) complexes of tripodal tetradentate ligands are isolated. Their characterization and use as catalysts for oxygen atom transfer between dimethyl sulfoxide (DMSO) and benzoin as well as the oxidation of pyrogallol are reported.

**DOI: 10.1002/ejic.201600694**